Journal of Power Sources 248 (2014) 253–264

Contents lists available at ScienceDirect

Journal of Power Sources

journal homepage: www.elsevier.com/locate/jpowsour

Direct methanol fuel cells with streamline graded structure under ultra-low fuel stoichiometry condition

Seunghun Jung*, Chao-Yang Wang

Electrochemical Engine Center (ECEC), Department of Mechanical and Nuclear Engineering, The Pennsylvania State University, University Park, PA 16802, USA

HIGHLIGHTS

- Severe non-uniformities in a DFMC are predicted under ultra-low fuel stoichiometry condition.
- This paper identifies the controlling parameters of the methanol transport in a DMFC.
- Two strategies called 'streamline graded structures (SGSs)' to mitigate non-uniformity are proposed.
- Computational results show SGS models have 10% improved performance compared to the baseline model.

ARTICLE INFO

Article history:
Received 29 June 2013
Received in revised form
16 September 2013
Accepted 19 September 2013
Available online 1 October 2013

Keywords:
Direct methanol fuel cell
Modeling
Non-uniformity
Graded structure

ABSTRACT

Operating a direct methanol fuel cell (DMFC) with ultra-low fuel stoichiometry is desirable to build a compact portable power system. Through 3D computational modeling with statistical analysis, severe non-uniformity of fuel concentration leading to high methanol crossover in the inlet region and poor fuel supply in the outlet region is predicted under ultra-low fuel stoichiometry condition, which causes large voltage loss or even cell shut-down. After identifying controlling parameters of methanol transport, this paper proposes streamline-graded structures (SGS) of the anode channel to mitigate anode fuel distribution non-uniformity and to boost cell performance and fuel efficiency together. Computational results show that streamline-graded structures achieve about 10% of voltage gain and 3% of fuel efficiency improvement compared to the conventional DMFC design by mitigating anode non-uniformity.

1. Introduction

In order to develop a compact, portable direct methanol fuel cell (DMFC) system, there are several objectives to achieve, such as high energy density, small system size and high fuel efficiency. First, energy density of the DMFC system must be increased by using highly concentrated fuel. Many DMFCs carry a diluted fuel solution which consists of water and methanol. Although cell operation with dilute solution has benefits of reducing methanol crossover and increasing cell voltage, it is not optimal for development of portable DMFCs because dilute solution lowers energy density of the entire DMFC system. As water is produced in the cathode catalyst layer by oxygen reduction reaction (ORR), it is theoretically possible to achieve a water-neutral condition to operate a DMFC without external water supply to the anode side. Blum et al. [1] first proposed this water-neutral condition and they concluded that carrying pure liquid methanol is theoretically possible when the water transfer coefficient (α) is equal to $-1/6$. However, supplying pure methanol to a DMFC causes severe methanol crossover and it is difficult to uniformly supply fuel to a DMFC with low fuel stoichiometry. Even though a DMFC system carries a pure methanol tank, it must dilute pure methanol internally with produced water.

Balance of plant (BOP), occupying a large volume of a DMFC system, should be reduced also. The gas–liquid separator located at the anode outlet can be removed if CO_2 gas is vented through alternate routes. Conventional DMFCs use a pump to supply liquid fuel on the anode side. If anode flow rate is minimized, this pump size can be reduced and required power for pump operation can be reduced as well. Due to CO_2 production by methanol oxidation reaction (MOR) in the anode, a strong two-phase flow exists in the anode channel. This two-phase flow causes a large pressure drop by two-phase frictional loss and inertial loss. The CO_2 breathing type DMFC removes CO_2 directly to the ambient and almost pure liquid

* Corresponding author. Battery R&D, LG Chem Research Park, 104-1, Moonji-dong, Yuseong-gu, Daejeon 305-380, South Korea. Tel.: +82 10 8443 5214; fax: +82 42 862 1981.
E-mail addresses: stratus76@hotmail.com, stratus760@gmail.com (S. Jung).

0378-7753/$ – see front matter © 2013 Elsevier B.V. All rights reserved.
http://dx.doi.org/10.1016/j.jpowsour.2013.09.080

flows in the anode channel, which reduces the required pumping power [2,3].

Maintaining ultra-low fuel stoichiometry is another way to construct a compact DMFC system and reduce manufacturing cost. When a DMFC operates with large fuel stoichiometry condition, redundant methanol which did not participate in anode reaction is lost to the cathode side by diffusion and electro-osmosis drag through the proton exchange membrane. This methanol crossover lowers the overall fuel efficiency. High fuel efficiency is particularly important for a portable system as it determines the total operational time of the system. The easiest way to minimize methanol crossover is to operate a DMFC with ultra-low fuel stoichiometry.

$$\nabla\cdot\left(\gamma\rho\vec{u}Y^{k}\right) = \nabla\cdot\left[\rho_{l}D^{k}_{l,\mathrm{eff}}\nabla Y^{k}_{l}+\rho_{g}D^{k}_{g,\mathrm{eff}}\nabla Y^{k}_{g}\right] - \nabla\cdot\left[\left(Y^{k}_{l}-Y^{k}_{g}\right)\vec{j}_{l}\right]+S^{k} \tag{1}$$

When the vapor–liquid equilibrium of methanol is assumed in the anode by Henry's law, gas and liquid methanol concentration are related as

$$c^{\mathrm{MeOH}}_{l} = c^{\mathrm{MeOH}}_{g}k^{\mathrm{MeOH}}_{H} \tag{2}$$

The following relationship can be established by multi-phase mixture model theory.

$$\rho Y^{\mathrm{MeOH}} = \rho_{l}Y^{\mathrm{MeOH}}_{l}s+\rho_{g}Y^{\mathrm{MeOH}}_{g}(1-s) \quad \text{where} \begin{cases} \rho Y^{\mathrm{MeOH}} = c^{\mathrm{MeOH}}M^{\mathrm{MeOH}} \\ \rho_{l}Y^{\mathrm{MeOH}}_{l} = c^{\mathrm{MeOH}}_{l}M^{\mathrm{MeOH}} \\ \rho_{g}Y^{\mathrm{MeOH}}_{g} = c^{\mathrm{MeOH}}_{g}M^{\mathrm{MeOH}} \end{cases} \tag{3}$$

And, theoretically, it is ideal to operates a DMFC near anode limiting current density regime where methanol crossover is almost zero, which enables the cell to achieve maximum performance with maximum fuel efficiency. It is, however, not easy to achieve this ideal operating condition because fuel concentration may distribute in three dimensions non-uniformly.

When a DMFC operates at very low fuel flow rate, convectional effect of methanol transport in the channel direction becomes weak. Instead, diffusive effect of methanol transport through the membrane electrode assembly becomes stronger and large amount of methanol may diffuse through the proton exchange membrane in the inlet region, causing severe methanol crossover there. In contrast, the outlet region may suffer from fuel depletion, which also degrades cell performance by increasing mass transport overpotential. Therefore, when liquid fuel is supplied from the inlet at ultra-low flow rate, some regions will operate with excessive fuel and some regions may suffer from fuel shortage. This is called 'fuel concentration non-uniformity'. Fuel concentration non-uniformity eventually leads to current density non-uniformity, temperature non-uniformity, and even cell shut-down. All of those non-uniformities are called 'anode non-uniformity'. It can be easily conjectured that the anode non-uniformity has a strong influence on the overall cell performance and fuel efficiency.

In this paper, we mathematically investigate the anode non-uniformity as well as its consequences on cell performance when a DMFC operates at ultra-low fuel stoichiometry. After identifying that, strategies of mitigating anode non-uniformity are introduced in order to improve both cell performance and fuel efficiency required for portable power sources.

2. Physics model

In order to analyze transport phenomena in a DMFC, previously developed multi-D DMFC model [4–6] is applied to the present study. Governing equations and constitutive relationships are summarized in Tables 1 and 2, respectively. Coupled PDEs (mass, momentum, species, proton transport, electron transport, and energy) are solved together with source terms. Cell dimension and simulation parameters are presented in Tables 3 and 4, respectively. As the present study focuses on methanol transport, the methanol transport equation for the multi-D model is revisited here. A general form of multi-phase species equation by M^2 model [7] can be expressed as follows:

Combining Eq. (2) and Eq. (3), methanol mass fraction can be found as follows

$$Y^{\mathrm{MeOH}} = \frac{\rho_{l}}{\rho}\left(s+\frac{1-s}{k^{\mathrm{MeOH}}_{H}}\right)Y^{\mathrm{MeOH}}_{l} \tag{4}$$

Therefore, the methanol transport equation can be reformed from Eq. (1) as follows:

$$\nabla\cdot\left(\rho\vec{u}Y^{\mathrm{MeOH}}_{l}\right) = \nabla\cdot\left[\rho_{l}\left(D^{\mathrm{MeOH}}_{l,\mathrm{eff}}+\frac{D^{\mathrm{MeOH}}_{g,\mathrm{eff}}}{k^{\mathrm{MeOH}}_{H}}\right)\nabla\cdot Y^{\mathrm{MeOH}}_{l}\right] - \nabla\cdot\left[\left(Y^{\mathrm{MeOH}}_{l}-Y^{\mathrm{MeOH}}_{g}\right)\vec{j}_{l}\right]+S^{\mathrm{MeOH}} \tag{5}$$

The first term on the right hand side in Eq. (5) expresses the two-phase molecular diffusion. Since molecular diffusion of methanol is carried out by both liquid phase and gas phase, we define two-phase molecular diffusivity of methanol as follows:

$$D^{\mathrm{MeOH}}_{\mathrm{eff}} = \frac{\rho_{l}}{\rho}\left(D^{\mathrm{MeOH}}_{l,\mathrm{eff}}+\frac{D^{\mathrm{MeOH}}_{g,\mathrm{eff}}}{k^{\mathrm{MeOH}}_{H}}\right) = \frac{\rho_{l}}{\rho}\left(D^{\mathrm{MeOH}}_{l}s^{n}+\frac{D^{\mathrm{MeOH}}_{g}(1-s)^{n}}{k^{\mathrm{MeOH}}_{H}}\right)\varepsilon^{n} \tag{6}$$

As the value of k^{MeOH}_{H} is about 1191 in the room temperature, $D^{\mathrm{MeOH}}_{l,\mathrm{eff}}$ and $D^{\mathrm{MeOH}}_{g,\mathrm{eff}}/k^{\mathrm{MeOH}}_{H}$ becomes similar order of magnitude. Note that two-phase molecular diffusivity of methanol is a strong function of both operating condition (liquid saturation) and material property (porosity). The liquid saturation shown above equation is defined as follows [7]:

$$s = \frac{V_{l}}{V_{\mathrm{pore}}} = 1-\frac{V_{g}}{V_{\mathrm{pore}}} = \frac{\rho_{g}Y^{H_2O}-\rho_{g}Y^{H_2O}_{g}}{\rho_{l}Y^{H_2O}_{l}-\rho_{l}Y^{H_2O}+\rho_{g}Y^{H_2O}-\rho_{g}Y^{H_2O}_{g}} \tag{7}$$

And porosity is defined as,

$$\varepsilon = \frac{V_{\mathrm{pore}}}{V} = \frac{V_{\mathrm{pore}}}{V_{g}+V_{l}+V_{\mathrm{pore}}} \tag{8}$$

The second term in Eq. (5) explains methanol transport by capillary force which becomes significant when the anode flow rate is large or methanol concentration is high. As the present study

Table 1
Governing equations of the multi-D DMFC model.

	Conservation equations	Source terms
Mass	$\nabla\cdot(\rho\vec{u}) = S^m$	$S^m_{\text{acl}} = M^{\text{MeOH}}S^{\text{MeOH}} + M^{\text{H}_2\text{O}}S^{\text{H}_2\text{O}} + \frac{j}{6F}M^{\text{CO}_2}$ $S^m_{\text{ccl}} = M^{\text{H}_2\text{O}}S^{\text{H}_2\text{O}} + M^{\text{O}_2}S^{\text{O}_2} + \frac{j_{\text{xover}}}{6F}M^{\text{CO}_2}$
Momentum	$\nabla\cdot(\rho\vec{u}\vec{u}) = -\nabla p + \nabla\cdot\vec{\tau} + S^{\text{u}}$	$S^{\text{u}} = -\frac{\mu}{K}\vec{u}$ (in porous media domain)
Water transport	$\nabla\cdot(\gamma\rho\vec{u}Y^{\text{H}_2\text{O}}) = \nabla\cdot[\rho D_{\text{capill}}\nabla Y^{\text{H}_2\text{O}}] + S^{\text{H}_2\text{O}}$	$S^{\text{H}_2\text{O}}_{\text{acl}} = -\frac{j}{6F}M^{\text{H}_2\text{O}} - \frac{j}{F}\alpha M^{\text{H}_2\text{O}}$ $S^{\text{H}_2\text{O}}_{\text{ccl}} = \frac{j}{2F}M^{\text{H}_2\text{O}} + \frac{j_{\text{xover}}}{2F}M^{\text{H}_2\text{O}} + \frac{j}{F}\alpha M^{\text{H}_2\text{O}}$
Methanol transport	$\nabla\cdot(\gamma\rho\vec{u}Y^{\text{MeOH}}_{\text{l}}) = \nabla\cdot[\rho D^{\text{MeOH}}_{\text{eff}}\nabla\cdot Y^{\text{MeOH}}_{\text{l}}] + S^{\text{MeOH}}$	$S^{\text{MeOH}}_{\text{acl}} = -\frac{j}{6F}M^{\text{MeOH}} - \frac{j_{\text{xover}}}{6F}M^{\text{MeOH}}$
Oxygen transport	$\nabla\cdot(\gamma\rho\vec{u}Y^{\text{O}_2}) = \nabla\cdot\left[\rho\left(\frac{\rho_g}{\rho}D^{\text{O}_2}_{\text{g,eff}}\right)\nabla Y^{\text{O}_2}\right] + \nabla\cdot[Y^{\text{O}_2}\vec{j}_{\text{l}}] + S^{\text{O}_2}$	$S^{\text{O}_2}_{\text{ccl}} = -\frac{j}{4F}M^{\text{O}_2} - \frac{j_{\text{xover}}}{4F}M^{\text{O}_2}$
Proton	$0 = \nabla\cdot(\kappa_{\text{e,eff}}\nabla\phi_{\text{e}}) + S^{\phi}_{\text{e}}$	$S^{\phi}_{\text{e,acl}} = j$ $S^{\phi}_{\text{e,ccl}} = -j_{\text{c}} + j_{\text{xover}}$
Electron	$0 = \nabla\cdot(\kappa_{\text{s,eff}}\nabla\phi_{\text{s}}) + S^{\phi}_{\text{s}}$	$S^{\phi}_{\text{s,acl}} = -j$ $S^{\phi}_{\text{s,ccl}} = j_{\text{c}} - j_{\text{xover}}$
Energy	$\nabla\cdot(\rho c_p\vec{u}T) = \nabla\cdot(k_{\text{eff}}\nabla T) + S^{\text{T}}$	$S^{\text{T}}_{\text{sensible,acl}} = j\left(\eta + T\frac{dU^0}{dT}\right) + \frac{i^2}{\kappa_{\text{eff}}}$ $S^{\text{T}}_{\text{sensible,mem}} = \frac{i^2}{\kappa_{\text{eff}}}$ $S^{\text{T}}_{\text{sensible,ccl}} = j\left(\eta + T\frac{dU^0}{dT}\right) + \frac{i^2}{\kappa_{\text{eff}}} + j_{\text{xover}}\left(\eta + T\frac{dU^0}{dT}\right)$ $S^{\text{T}}_{\text{latent}} = \nabla\cdot(h^o_{\text{lg}}\rho_{\text{l}}\vec{u}_{\text{l}})$

focuses on ultra-low stoichiometry condition, the anode becomes gaseous and the methanol capillary term can be neglected. Finally, the methanol transport equation becomes,

$$\nabla\cdot\left(\rho\vec{u}Y^{\text{MeOH}}_{\text{l}}\right) = \nabla\cdot\left[\rho D^{\text{MeOH}}_{\text{eff}}\nabla\cdot Y^{\text{MeOH}}_{\text{l}}\right] + S^{\text{MeOH}} \tag{9}$$

Fig. 1 schematically shows methanol transport in the anode. Supplied methanol from the channel inlet spreads out through the anode porous media and the remaining amount moves out of the channel outlet. Methanol is convection-dominantly transported from the channel to the surface of the gas diffusion layer. Then, methanol is diffusively transported to the catalyst layer through the porous media. Note that the ratio of channel width and membrane width strongly affects diffusive mass transport between the surface of the gas diffusion layer and the catalyst layer. Considering the above two mass transport mechanisms, methanol transported from the channel to the catalyst layer can be simply expressed as Eq. (10).

Table 2
Constitutive relationships and parameters for the multi-D DMFC model.

Parameters	Expression	Reference
Relative permeability	$k_{\text{r,l}}=s^{\text{n}}$; $k_{\text{r,g}}=(1-s)^{\text{n}}$	[14]
Methanol diffusivity (vapor)	$D^{\text{MeOH,H}_2\text{O}}_{\text{g}} = D^{\text{MeOH,CO}_2}_{\text{g}} = 1.96\times10^{-5}\left(\frac{T}{328.15}\right)^{1.823}\frac{101300.0}{p}$	[15]
Water diffusivity (vapor)	$D^{\text{H}_2\text{O,CO}_2}_{\text{g}} = 2.01\times10^{-5}\left(\frac{T}{307}\right)^{1.823}\frac{101300.0}{p}$	[16]
Methanol diffusivity (liquid)	$D^{\text{MeOH,H}_2\text{O}}_{\text{l}} = 1.4\times10^{-9}\left(\frac{647.3-298.15}{647.3-T}\right)^{6}$	[20]
Oxygen diffusivity (gas)	$D^{\text{O}_2}_{\text{g}} = 3.57\times10^{-5}\left(\frac{T}{352}\right)^{1.823}\frac{101300.0}{p}$	[16]
Water content in Nafion-membrane	$\lambda = \begin{cases} 22 & (s>0.3) \\ 14+8s/0.3 & (s\le 0.3) \end{cases} 0.043 + 17.81RH - 39.85RH^2 + 36.0RH^3$ (vapor)	[17,18]
Water diffusivity in Nafion-membrane	$D^{\text{H}_2\text{O}}_{\text{mem}} = 4.80\times10^{-11}\exp\left[2416\left(\frac{1}{303}-\frac{1}{T}\right)\right]$	Calibrated based on [17]
Methanol diffusivity in Nafion-membrane	$D^{\text{MeOH}}_{\text{mem}} = 1.5\times10^{-10}\exp\left[2416\left(\frac{1}{303}-\frac{1}{T}\right)\right]$	Calibrated based on [17]
Henry's constant	$k^{\text{MeOH}}_{\text{H}} = \frac{160.0}{101.235}\exp\left[4210\left(\frac{1}{T}-\frac{1}{298.15}\right)\right]\frac{R}{T}$	Fitted data
Water EOD coefficient in Nafion-membrane	$n^{\text{H}_2\text{O}}_{\text{d}} = \begin{cases} \left[\frac{\lambda-14}{8}\right]\left(n^{\text{H}_2\text{O}}_{\text{d,ref}}-1\right)+1 & (\text{for } \lambda\ge 14) \\ 1.0 & (\text{for } \lambda<14) \end{cases}$	[19], [21]
Water reference EOD coefficient in Nafion-membrane	$n^{\text{H}_2\text{O}}_{\text{d,ref}} = 1.6767 + 0.0155(T-273) + 8.9074\times10^{-5}(T-273)^2$	[19]
Methanol drag coefficient in Nafion-membrane	$n^{\text{MeOH}}_{\text{d}} = n^{\text{H}_2\text{O}}_{\text{d}}\frac{c^{\text{MeOH}}}{c_{\text{tot}}}$	[5]
Ion conductivity of Nafion-membrane	k_{mem}=0.1(S cm^{-1})@60°C (fully hydrated)	
Effective water vapor diffusivity	$D^{\text{H}_2\text{O}}_{\text{g,eff}} = D^{\text{H}_2\text{O}}_{\text{g}}(1-s)^{\text{n}}\varepsilon^{\text{n}}$	
J-Leverett function	$J(s) = \begin{cases} -1.263s^3 + 1.669s^2 - 0.966s + 0.56 & (\text{when } \theta_c<90^o) \\ 1.263s^3 - 2.120s^2 + 1.417s & (\text{when } \theta_c>90^o) \end{cases}$	

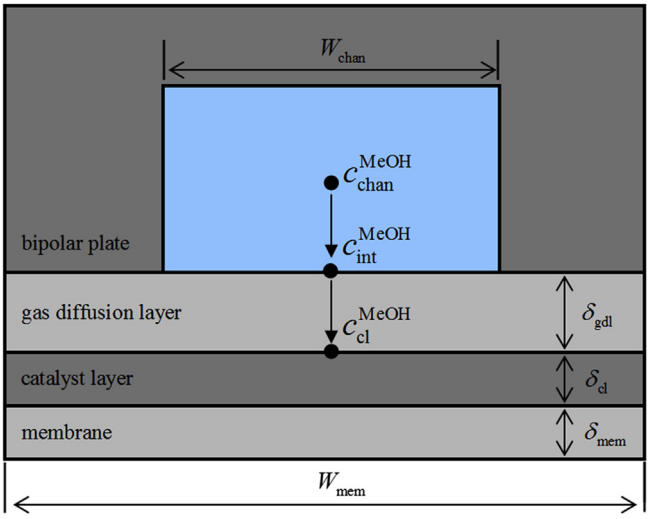

Fig. 1. Schematic of methanol transport by convection and diffusion in the anode of a DMFC.

$$\dot{m}^{MeOH} = \frac{A_{mem}\left\{c^{MeOH}_{chan} - c^{MeOH}_{acl}\right\}M_{MeOH}}{\frac{1}{h_m A_r} + \frac{\delta_{gdl}}{D^{MeOH}_{eff}\left\{1-2^{-1/n}(1-A_r)\right\}}} \quad (10)$$

where $A_r = \frac{W_{chan}}{W_{mem}}$ (openning ratio)

Note $D^{MeOH}_{eff}\{1-2^{-1/n}(1-A_r)\}$ in the above equation is a semi-empirical equation derived for considering mass transport from the surface of the anode gas diffusion layer to the catalyst layer.

The effective resistance which consists of convective resistance and diffusive resistance expresses the total resistance controlling methanol transport as follows:

$$R_{eff} = R_{conv} + R_{diff} = \frac{1}{h_m A_r} + \frac{\delta_{gdl}}{D^{MeOH}_{eff}\left\{1-2^{-1/n}(1-A_r)\right\}} \quad (11)$$

Convective resistance (R_{conv}) is determined by opening ratio (A_r) and convective mass transfer coefficient which is a function of flow rate (Re_D) as follows [8]:

$$h_m = Sh\frac{D^{MeOH}_{chan}}{H} = 1.86\left(\frac{Re_{D_H}Sc}{L\cdot D_H}\right)^{1/3}\left(\frac{D^{MeOH}_{chan}}{H}\right) \text{ where } \begin{cases} Sc = \frac{\mu}{\rho D^{MeOH}_{chan}} \\ Re_{D_H} = \frac{\rho u D_H}{\mu} \end{cases} \quad (12)$$

Under ultra-low fuel stoichiometry condition, methanol diffusive resistance, R_{diff} becomes the dominant transport resistance, which is a function of both material property (porosity) and channel geometry (A_r). Dependence of the methanol diffusive resistance on porosity, channel geometry and temperature is presented in Fig. 2. Diffusive resistance exponentially increases when porosity decreases. Opening ratio and temperature also affect the diffusive resistance, albeit less strongly than porosity.

The effect of methanol concentration in the anode catalyst layer on the cell performance is considered as follows [9–11]:

$$j_a = \frac{a_s i_{0,a} c^{MeOH}_{acl}\exp\left(\frac{\alpha_a F}{RT}\eta_a\right)}{c^{MeOH}_{acl} + k_a\exp\left(\frac{\alpha_a F}{RT}\eta_a\right)} \text{ where } \eta_a = \Phi_s - \Phi_e - U^0_a \quad (13)$$

Eq. (13) explains the reaction order shift from 1st to 0th when methanol concentration becomes higher than the threshold value. On the cathode side, oxygen reduction reaction (ORR) is assumed to be proportional to oxygen concentration.

$$j_c = a_s i_{0,c} c^{O_2}_{ccl}(1-s)^n\exp\left(-\frac{\alpha_c F}{RT}\eta_c\right) \text{ where } \eta_c = \Phi_s - \Phi_e - U^0_c \quad (14)$$

Fig. 3(a) shows the base model geometry used in the present study. Micro-porous layers are inserted between gas diffusion layer and catalyst layer on both anode and cathode side. It is known that saturation jump occurs between different porous media, and the micro-porous layer plays an important role in controlling water management in a DMFC by developing saturation jump [12,13]. Previous study [6] mathematically revealed that the anode micro-porous layer acts as a barrier which preventing liquid in the anode from flowing to the cathode, which helps to lower methanol crossover and water transfer coefficient, whereas the cathode micro-porous layer reserves liquid in the cathode catalyst layer, increasing water back-diffusion. Multi-D saturation jump model is applied to the present DMFC model which has four interfaces between different porous media. The anode becomes gaseous in the channel direction since CO_2 is accumulated, whereas the cathode becomes wetter in the channel direction since produced water is accumulated according to the operational condition (cathode inlet gas humidity). In addition, the region under the anode land is gaseous due to CO_2 removal blockage there, whereas the region under the cathode land is wet due to water removal blockage. The energy equation is solved in order to examine temperature distribution which may be affected by anode non-uniformity in the present study.

The present multi-D model is implemented into a commercial CFD package, STAR-CD™ through the user subroutine capability. AMG (algebraic multi-grid method) based on finite volume method (FVM) is used for discretization and SIMPLE algorithm is applied for solving governing equations. It is considered that convergence is achieved when the residuals reach 10^{-8}.

3. Results and discussion

3.1. Anode fuel non-uniformity under ultra-low flow stoichiometry

The effect of anode stoichiometry on the cell performance and fuel non-uniformity is investigated using the multi-D simulation. Methanol concentration distribution in the anode catalyst layer for stoichiometry 2.4 and 1.4 are presented in Fig. 4(a) and 4(b), respectively. Under ultra-low anode stoichiometry condition ($\xi_a = 1.4$), methanol is concentrated in the inlet region and the outlet half region suffers from fuel shortage. Current density or

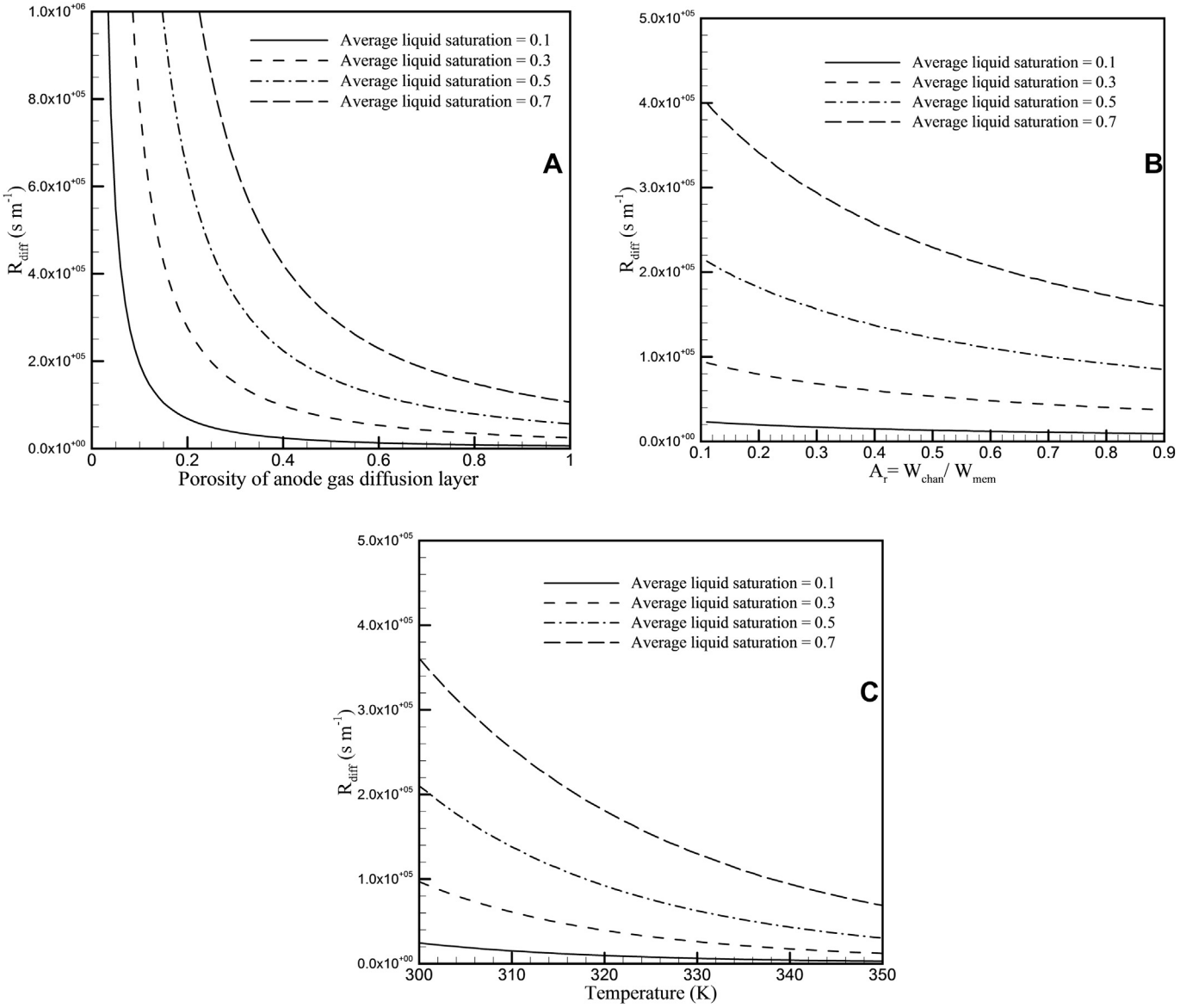

Fig. 2. Diffusive resistance according to (a) GDL porosity (ε), (b) opening ratio (A_r), and (c) Temperature (K).

anode reaction rate is strongly affected by methanol concentration when methanol concentration is insufficient. For the same operating current condition (150 mA cm^{-2}), the outlet half region has lower current density than the average value whereas the inlet half region has high current density compared to the average value, which means large anode non-uniformity of current density (see Fig. 5). Crossover current density which is calculated by Eq. (15) is presented in Fig. 6.

$$i_{\text{xover}} = 6FN_{\text{mem}}^{\text{MeOH}}$$
$$\text{where } N_{\text{mem}}^{\text{MeOH}} = D_{\text{mem}}^{\text{MeOH}}\frac{c_{\text{acl}}^{\text{MeOH}}}{\delta_{\text{mem}}} + n_{\text{d}}^{\text{MeOH}}\frac{i}{F} \quad (15)$$

As methanol crossover consists of diffusion through the membrane and electro-osmosis by electric current, methanol crossover is concentrated in the inlet region where both current density and methanol concentration are high under ultra-low anode stoichiometry condition. When fuel stoichiometry is large, methanol crossover becomes more uniform. Methanol crossover rate also affects temperature distribution. Examining heat source terms in the energy equation (see Table 1), crossover current density contributes to the heat generation on the cathode side. As methanol crossover is concentrated in the inlet region, the low anode stoichiometry case shows larger temperature gradient along the streamline direction compared to the large stoichiometry case (see Fig. 7(a) and 7(b)).

Although large anode flow stoichiometry assures better cell voltage due to lowered mass transport overpotential and good anode uniformity, it causes large methanol crossover rate and requires considerable fuel pumping power. In contrast, the cell may suffer from severe fuel shortage at the outlet region under ultra-low anode stoichiometry condition, which results in large anode overpotential and poor anode uniformity.

High temperature leads to better methanol diffusion in porous media due to the Arrhenius relationship of diffusivity as shown in Fig. 2(c). In addition, methanol oxidation reaction is also improved from Eq. (13). Therefore, high temperature generally leads to better cell performance. However, this may not be the case when

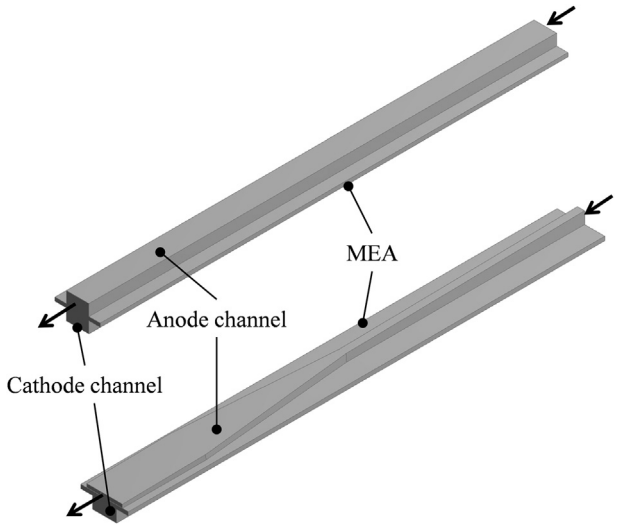

Fig. 3. Three-dimensional geometry of DMFC models which have seven porous layers (anode diffusion layer | anode micro-porous layer | anode catalyst layer | proton exchange membrane | cathode catalyst layer | cathode micro-porous layer | cathode diffusion layer), (a) Base DMFC (upper model), (b) SGS DMFC with tapered channel (lower model).

the cell operates at ultra-low fuel stoichiometry. High temperature increases not only the effective diffusivity in the anode porous media but also methanol diffusivity of the proton exchange membrane, which is not desired for fuel management since it may exacerbate large methanol crossover. Effect of temperature on fuel distribution can be examined by comparing Fig. 4(b) with (c). As a large amount of methanol is transported to the anode catalyst layer in the inlet region due to increased effective methanol diffusivity, much more methanol is consumed there by both methanol oxidation reaction and methanol crossover when the temperature is high under ultra-low anode stoichiometry condition. Therefore, the outlet half region suffers from fuel shortage and poor anode kinetics, which worsens anode non-uniformity (see Figs. 5–7). It is predicted that the cell may shut down with severe anode non-uniformity when the cell temperature exceeds 70 °C under ultra-low anode stoichiometry in the present study. Therefore, excessive cell temperature should be managed under ultra-low anode stoichiometry condition. In order to operate the cell at high temperature while maintaining low methanol crossover under ultra-low anode flow stoichiometry condition, a hydrocarbon membrane with low methanol diffusivity can be selected as the proton exchange membrane instead of a fluorocarbon membrane.

3.2. Mitigation of non-uniformity by controlling methanol transport resistance

It is clear that non-uniform fuel distribution leads to other anode non-uniformities such as current density, crossover current density, and temperature as discussed. In addition, severe anode non-uniformity leads to poor cell voltage and poor fuel efficiency. Therefore, if we mitigate methanol concentration non-uniformity, we can simultaneously improve cell performance and fuel efficiency. Cell operation under ultra-low anode stoichiometry can thus be achieved without sacrificing cell performance. In order to mitigate non-uniform fuel distribution, we should investigate clues for this in the methanol transport mechanism discussed previously.

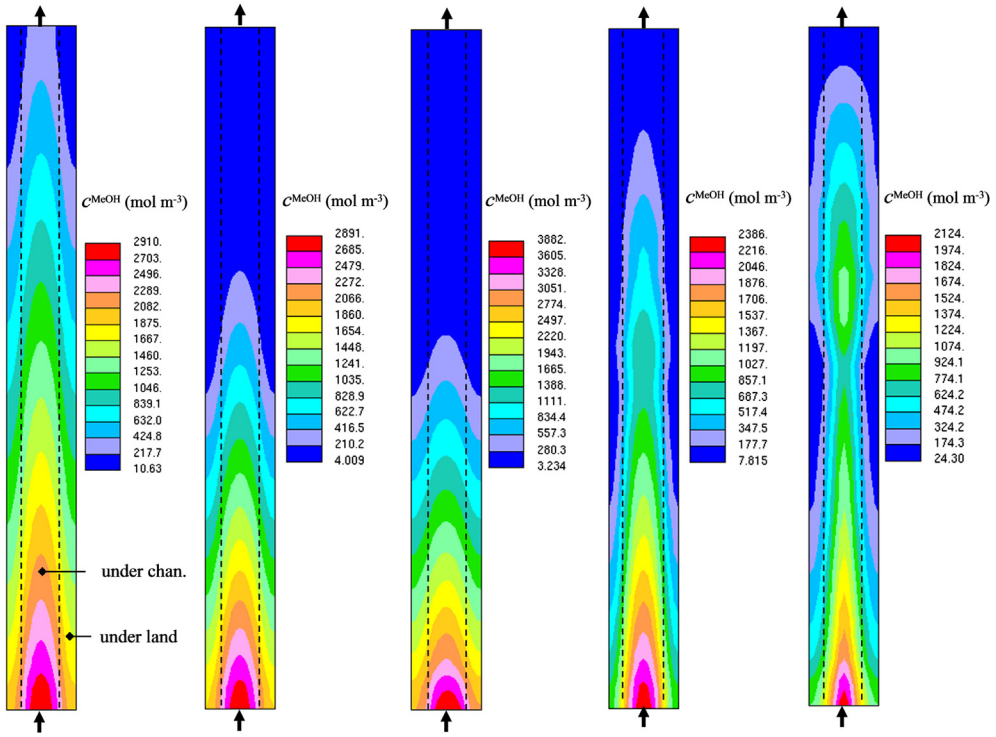

Fig. 4. Methanol concentration distribution in the anode catalyst layer of DMFCs operating at $\bar{i}$ = 150 mA cm^{-2}, (a) Base model (T_{cell} = 313 K, ζ_a = 2.4, ζ_c = 2.4), (b) Base model (T_{cell} = 313 K, ζ_a = 1.4, ζ_c = 2.0), (c) Base model (T_{cell} = 323 K, ζ_a = 1.4, ζ_c = 2.0), (d) SGS model with variable porosity type A (T_{cell} = 313 K, ζ_a = 1.4, ζ_c = 2.0), (e) SGS model with tapered channel (T_{cell} = 313 K, ζ_a = 1.4, ζ_c = 2.0).

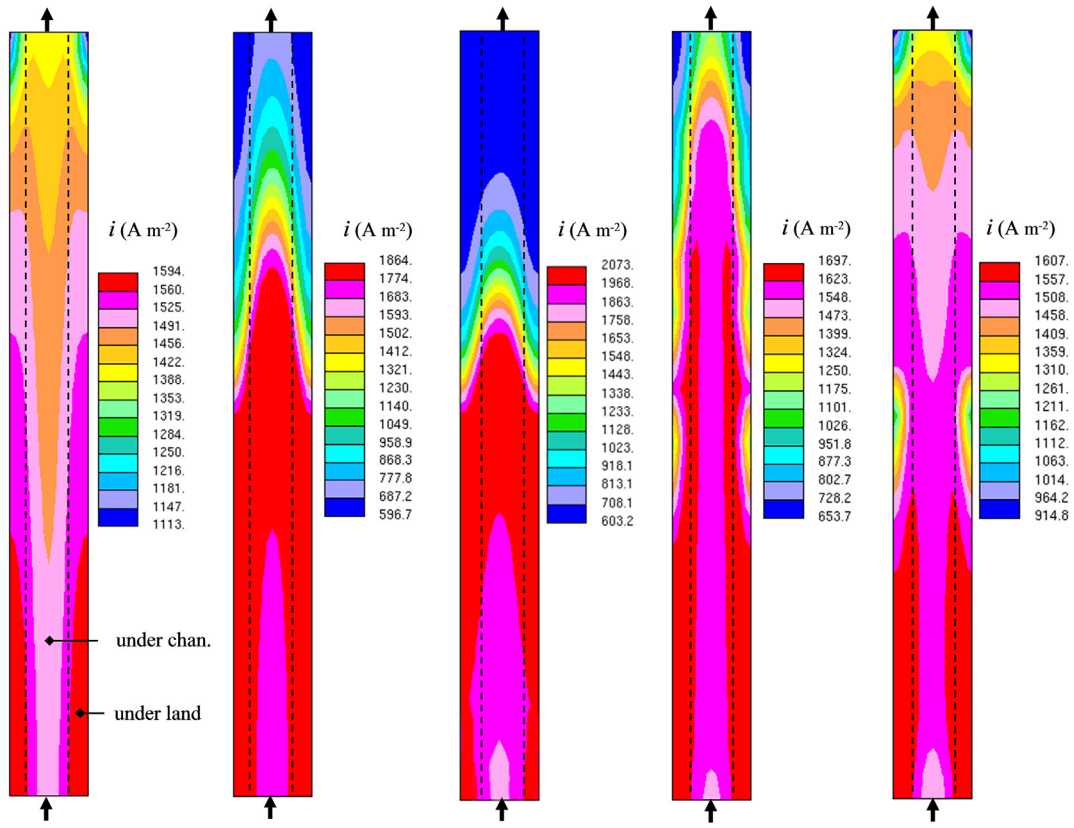

Fig. 5. Current density distribution of DMFCs operating at $\bar{i}$ = 150 mA cm^{-2}, (a) Basel model (T_{cell} = 313 K, ζ_a = 2.4, ζ_c = 2.4), (b) Base model (T_{cell} = 313 K, ζ_a = 1.4, ζ_c = 2.0), (c) Base model (T_{cell} = 323 K, ζ_a = 1.4, ζ_c = 2.0), (d) SGS model with variable porosity type A (T_{cell} = 313 K, ζ_a = 1.4, ζ_c = 2.0), (e) SGS model with tapered channel (T_{cell} = 313 K, ζ_a = 1.4, ζ_c = 2.0).

It is shown that the effective resistance in Eq. (11) controls methanol transport in a DMFC. The conventional DMFC has almost uniform effective methanol transport resistance in the streamline direction, which results in large methanol concentration gradient in the streamline direction, i.e., methanol concentration non-uniformity (see Figs. 4–7). In order to build a more uniform methanol concentration distribution in the streamline direction, we should vary the effective methanol transport resistance itself. The inlet region where large methanol crossover occurs must have significant methanol transport resistance to reduce methanol transport. In contrast, the outlet region must have minimal methanol transport resistance to enhance methanol transport. Hereafter, we call this concept the streamline-graded structure (SGS). Although cell temperature and methanol concentration also affect the effective methanol diffusivity, they are not design parameters but operating conditions. Opening ratio and porosity are important design parameters to construct SGS, and affect the effective methanol transport resistance as shown in Fig. 2.

The opening ratio affects not only convective transport but also diffusive transport. Narrow channel width (small A_r) in the inlet region reduces diffusive transport by increasing diffusion length. Deepening channel depth can be helpful for reducing convective effect and delaying methanol diffusion in inlet region. On the contrary, in the outlet half region where methanol concentration is low, a wide channel is beneficial due to short diffusion length, and shallow depth improves the convective effect. In summary, the final anode channel design has a three-dimensionally tapered shape as shown in Fig. 3(b).

Molecular methanol diffusivity (D_{mol}^{MeOH}) is a strong function of porosity. In order to get a linearly varying diffusivity in streamline direction as,

$$D_{mol}^{MeOH}(y) = D_{min}^{MeOH} + \left(\frac{D_{max}^{MeOH} - D_{min}^{MeOH}}{L}\right) y \tag{16}$$

Porosity of the anode gas diffusion layer can be set up as,

$$\varepsilon(y) = \left[\varepsilon_{min}^{n} + \left(\frac{\varepsilon_{max}^{n} - \varepsilon_{min}^{n}}{L}\right) y\right]^{\frac{1}{n}} \tag{17}$$

However, it is not easy to fabricate a material which has smoothly varying porosity as above. Instead, porosity can be distributed in a stepping shape as shown in Fig. 8.

3.3. Methanol transfer resistance

Liquid saturation in the anode of the multi-D model decreases along the channel due to CO_2 gas accumulation. Therefore, molecular methanol diffusivity, which is a strong function of liquid saturation, increases and methanol transport resistance decreases in the channel direction in the base model as shown in Fig. 9. SGS models show much greater resistance in the inlet region compared to the base model. Although each SGS model adopts different approach to control methanol transport, the resulting resistance is similar.

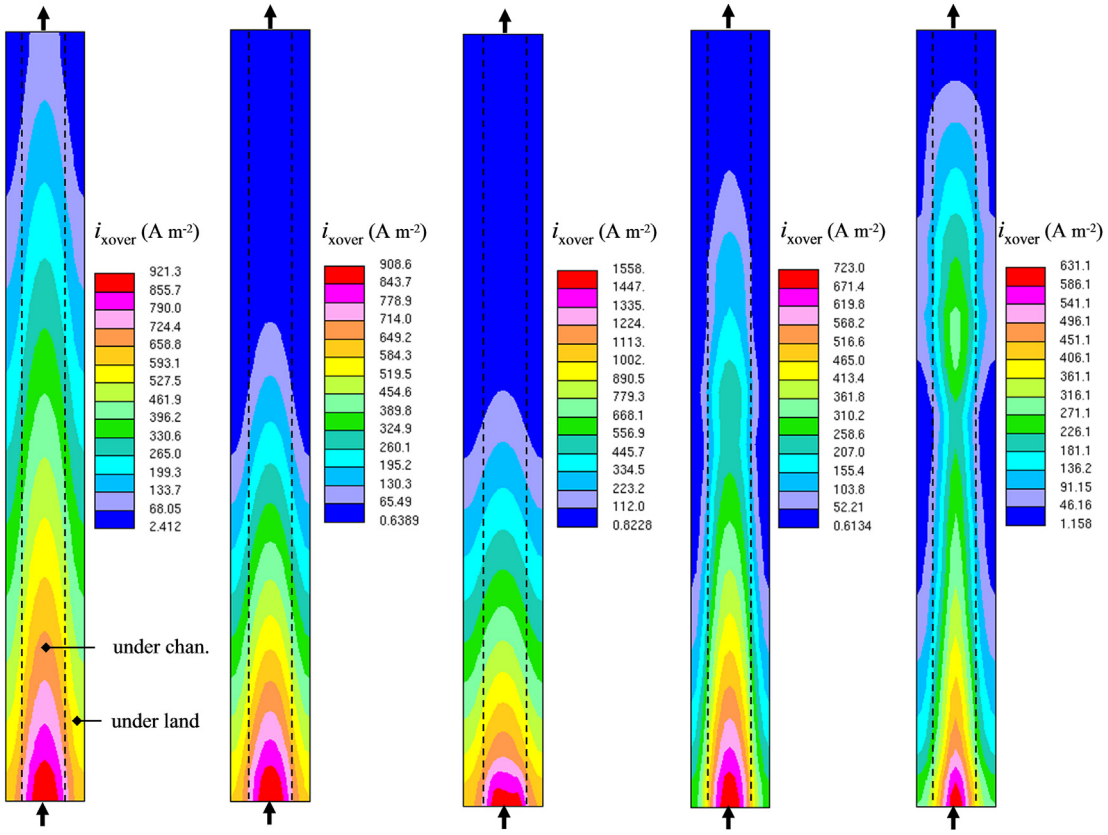

Fig. 6. Crossover current density distribution of DMFCs operating at $\bar{i}$ = 150 mA cm^{-2}, (a) Base model (T_{cell} = 313 K, ζ_a = 2.4, ζ_c = 2.4), (b) Base model (T_{cell} = 313 K, ζ_a = 1.4, ζ_c = 2.0), (c) Base model (T_{cell} = 323 K, ζ_a = 1.4, ζ_c = 2.0), (d) SGS model with variable porosity type A (T_{cell} = 313 K, ζ_a = 1.4, ζ_c = 2.0), (e) SGS model with tapered channel (T_{cell} = 313 K, ζ_a = 1.4, ζ_c = 2.0).

3.4. Methanol concentration distribution

It is important to avoid 1st-order methanol oxidation reaction in the anode catalyst layer for high uniformity of current density while maintaining sufficiently low methanol concentration near the anode catalyst layer to avoid severe methanol crossover which deteriorates both cell performance and fuel efficiency. This requirement eventually leads to achieving high uniformity of methanol concentration distribution, which is the main goal of the present study.

Methanol concentration in the anode channel direction is presented in Fig. 10. Contrary to the base model which shows large variation along the channel, SGS models show relatively uniform distribution of methanol concentration due to the effect of redistribution of methanol transport resistance. Compared to the base model (Fig. 4(b)), SGS models (Fig. 4(d) and (e)) shows increased methanol concentration in the outlet region while it is lowered in the inlet region. This mitigates anode non-uniformity that will reduce methanol crossover in the inlet region and risk of fuel shortage in the outlet region also.

3.5. Current density distribution

Calculation results of current density distribution in the channel direction of multi-D model are presented in Fig. 11. As the cathode side is same for all cases, different current density distribution comes from the anode side. The base model shows severe non-uniformity which is direct consequence of non-uniform distribution of methanol concentration.

In the base model, peak current occurs not just in the inlet region but around the center region in the channel direction due to large methanol crossover at the inlet. SGS models have improved uniformity, and peak current density is observed almost in the inlet region due to reduced methanol crossover. A contour plot of current density is shown in Fig. 5. Note that peak current density is observed under the land region in the inlet half where excessive methanol concentration causes severe methanol crossover leading to negative mixed potential. In the outlet half region where methanol concentration is low, peak current density is observed under the channel region where methanol concentration is high compared to the region under the land.

3.6. Crossover current density distribution

As the crossover current density is directly determined by methanol crossover rate that is a strong function of methanol concentration at interface between the anode catalyst layer and the proton exchange membrane (see Eq. (15)), calculation result of crossover current density distribution (Fig. 12) is very similar to methanol concentration distribution (Fig. 10). The base model has strong crossover current density in the inlet region, degrading cell performance by mixed potential. As SGS models have reduced current density in the inlet region, crossover current by EOD is lower than that of the base model there. In addition, lowered methanol concentration of SGS models also reduces crossover current by diffusion in the inlet region. Hence, SGS models have reduced overpotential in inlet region.

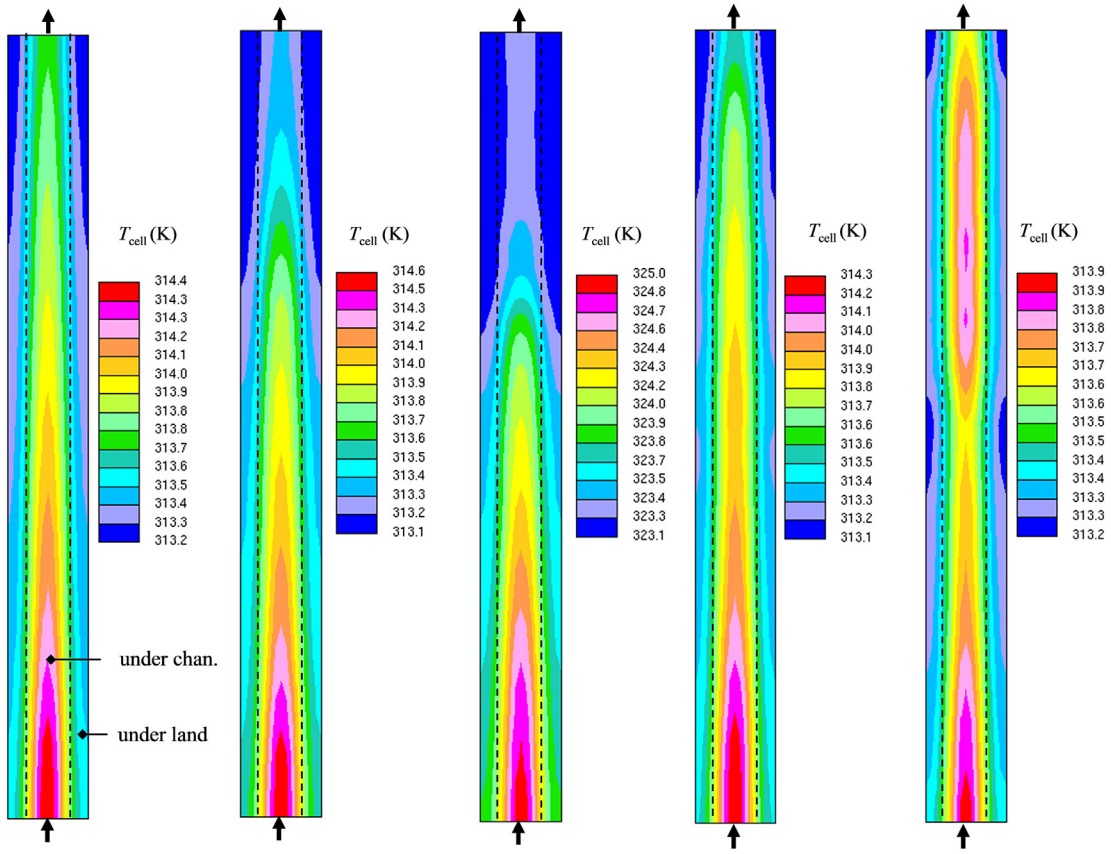

Fig. 7. Temperature distribution in membrane of DMFCs operating at $\bar{i}$ = 150 mA cm^{-2}, (a) Base model (T_{cell} = 313 K, ζ_a = 2.4, ζ_c = 2.4), (b) Base model (T_{cell} = 313 K, ζ_a = 1.4, ζ_c = 2.0), (c) Base model (T_{cell} = 323 K, ζ_a = 1.4, ζ_c = 2.0), (d) SGS model with variable porosity type A (T_{cell} = 313 K, ζ_a = 1.4, ζ_c = 2.0), (e) SGS model with tapered channel (T_{cell} = 313 K, ζ_a = 1.4, ζ_c = 2.0).

Average methanol crossover rate according to average operational current density is presented in Fig. 13. SGS models shows around 3% of fuel efficiency improvement compared to the base model.

3.7. Temperature distribution

It is important to maintain uniform temperature of the membrane to avoid local thermal degradation, especially in large cells. Major heat sources increasing cell temperature are current and

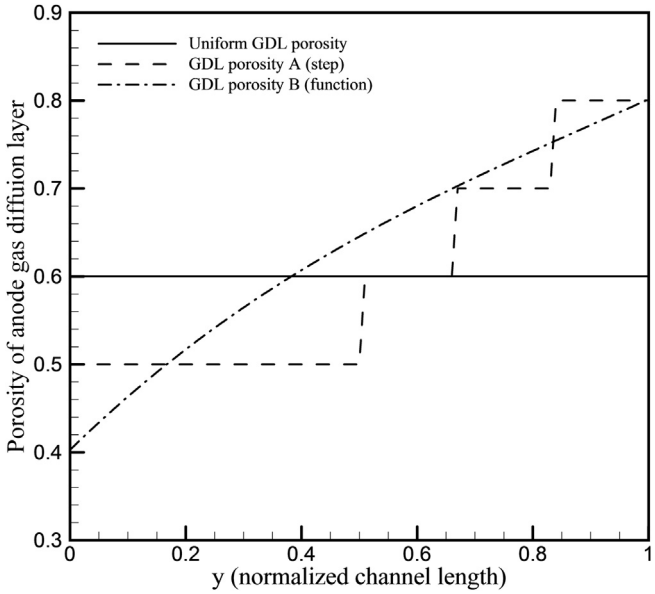

Fig. 8. Porosity distribution of the anode gas diffusion layer in the anode channel direction.

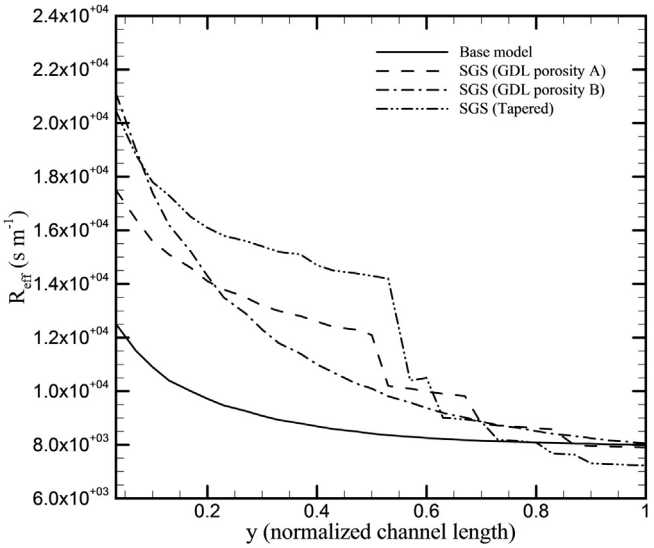

Fig. 9. Methanol transfer resistance distribution in the anode channel direction (T_{cell} = 313 K, $\bar{i}$ = 150 mA cm^{-2}, ξ_a = 1.4, ξ_c = 2.0).

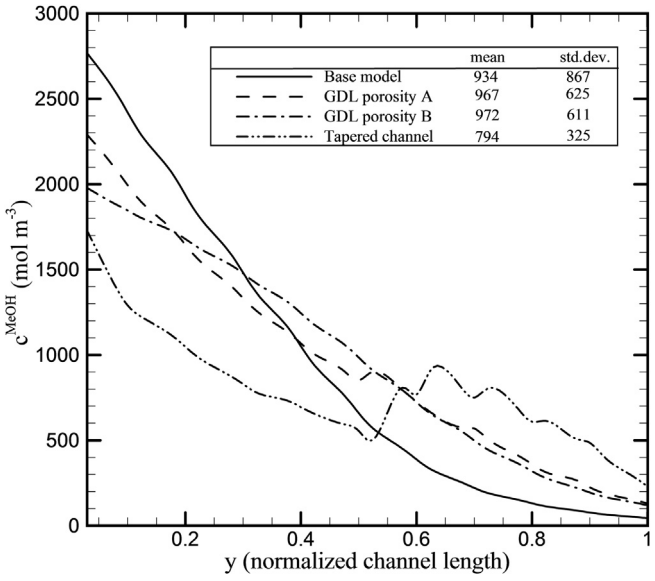

Fig. 10. Methanol concentration distribution in the anode channel direction (T_{cell} = 313 K, $\bar{i}$ = 150 mA cm^{-2}, ξ_a = 1.4, ξ_c = 2.0).

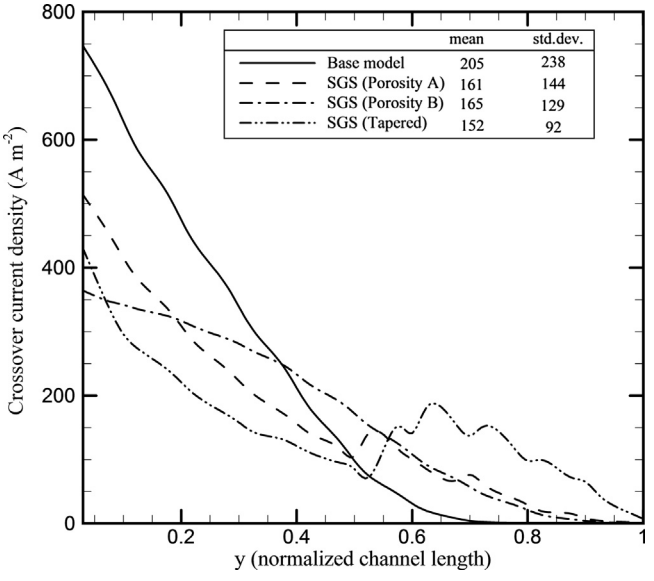

Fig. 12. Crossover current density distribution in the anode channel direction (T_{cell} = 313 K, $\bar{i}$ = 150 mA cm^{-2}, ξ_a = 1.4, ξ_c = 2.0).

crossover current. Therefore, non-uniform distribution of those currents leads to large temperature gradient in the cell. As Fig. 7 shows, SGS models have more uniform temperature distribution than the base model. The region under the channel at the inlet is the hottest area due to large methanol oxidation reaction and methanol crossover.

3.8. Overpotential and cell performance

Overpotentials of each model are summarized in Table 5. As all models share the same cathode, cathode overpotentials are almost the same for each case. SGS models show better performance than the base model and this performance improvement came from the reduced anode overpotential by delaying MOR order shift.

Finally, polarization curves are shown in Fig. 14. SGS models show improved performance. In addition, SGS models have somewhat extended limiting current density because saved fuel in the inlet region due to reduced MCO was utilized in the outlet region, preventing the cell from shutting down at high current operation.

4. Conclusion

It is found that DMFC which has conventional anode structure suffer from severe methanol crossover in the inlet region (low fuel efficiency) and methanol shortage in outlet region (low cell voltage) under ultra-low fuel stoichiometry condition. In addition, it is estimated that excessively high cell temperature degrades cell performance by severe methanol crossover in the inlet region.

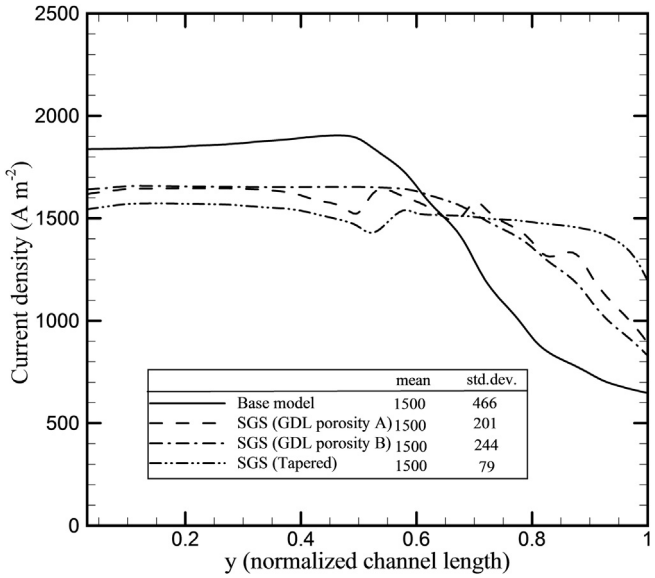

Fig. 11. Current density distribution in the anode channel direction (T_{cell} = 313 K, $\bar{i}$ = 150 mA cm^{-2}, ξ_a = 1.4, ξ_c = 2.0).

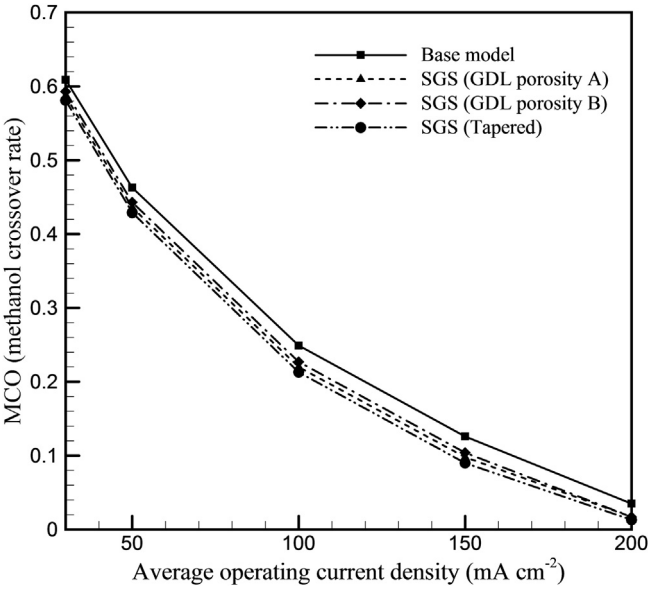

Fig. 13. Average methanol crossover rate according to average operating current density.

Table 3
Base cell geometry and material properties.

Description	Symbol	Value
Anode GDL thickness	δ_{adl}	270 μm
Anode MPL thickness	δ_{mpl}	30 μm
Anode CL thickness	δ_{acl}	62 μm
Membrane thickness	δ_{mem}	45 μm
Cathode CL thickness	δ_{ccl}	25 μm
Cathode MPL thickness	δ_{mpl}	30 μm
Cathode GDL thickness	δ_{cdl}	210 μm
GDL porosity	ε_{gdl}	0.6
MPL porosity	ε_{mpl}	0.4
CL porosity	ε_{cl}	0.4
GDL permeability	K_{gdl}	$2.0\text{x}10^{-12}$ m^2
MPL permeability	K_{mpl}	$5.0\text{x}10^{-14}$ m^2
CL permeability	K_{cl}	$1.0\text{x}10^{-13}$ m^2
Membrane permeability	K_{mem}	$4.0\text{x}10^{-20}$ m^2
GDL contact angel	θ_{gdl}	110°
MPL contact angel	θ_{mpl}	114°
CL contact angle	θ_{cl}	96°
Cell length	L_{cell}	75 mm
Channel width	W_{chan}	1 mm
Channel height	H_{chan}	0.5 mm
Land width	W_{land}	1 mm
Bipolar plate thickness	H_{bp}	0.5 mm

Table 4
Simulation parameters.

Description	Symbol	Value
Anode exchange current density	$i_{0,a}$	45.51 A m^{-2}
Cathode exchange current density	$i_{0,c}$	0.12 A m^{-2}
Anode catalyst ionomer		25 vol. %
Cathode catalyst ionomer		25 vol. %
Anode catalyst loading		4 mg cm^{-2}
Cathode catalyst loading		2 mg cm^{-2}
Surface tension	σ	0.0625 N m^{-1}
Inlet methanol concentration	c_{in}^{MeOH}	4000 mol m^{-3}
Pure liquid methanol concentration	c_{pure}^{MeOH}	24719 mol m^{-3}
Pure liquid water concentration	$c_{pure}^{H_2O}$	55556 mol m^{-3}
Total anode transfer coefficients	α_a	0.239
Total cathode transfer coefficients	α_c	0.875
Faraday constant	F	96487 C mol^{-1}
Universal gas constant	R	8.314 J mol^{-1}K^{-1}
Equivalent weight of dry membrane	EW	1.1 kg mol^{-1}

In order to overcome these problems occurring under ultra-low fuel stoichiometry conditions, the present study suggested streamline-graded structures (SGS) which are designed to boost cell performance and fuel efficiency by mitigating anode non-uniformity. Although the calculated results obtained from the present study showed that SGS models achieved about 10% improvement of voltage and 3% improvement of fuel efficiency, the better performance gain can be obtained through the optimization process which is not covered in this study. In addition, long-term stability of cell operation is not covered in the present study as the present 3D model is a steady-state model. As this stability issue is specially important for portable application of DMFCs, it will be covered through the transient model in the future.

Table 5
Calculation summary.

	ξ_a	ξ_c	T_{cell}	i (mA cm^{-2})	η_a (V)	η_c (V)	V_{cell} (V)	MCO (%)
Base model	1.4	2.0	313	150	0.444	0.274	0.408	12.0
	2.4	2.4	313	150	0.396	0.284	0.455	19.5
	1.4	2.0	323	150	0.477	0.306	0.345	16.5
SGS model (Porosity A)	1.4	2.0	313	150	0.413	0.277	0.443	9.7
SGS model (Porosity B)	1.4	2.0	313	150	0.415	0.276	0.441	9.9
SGS model (Tapered)	1.4	2.0	313	150	0.399	0.276	0.458	9.0

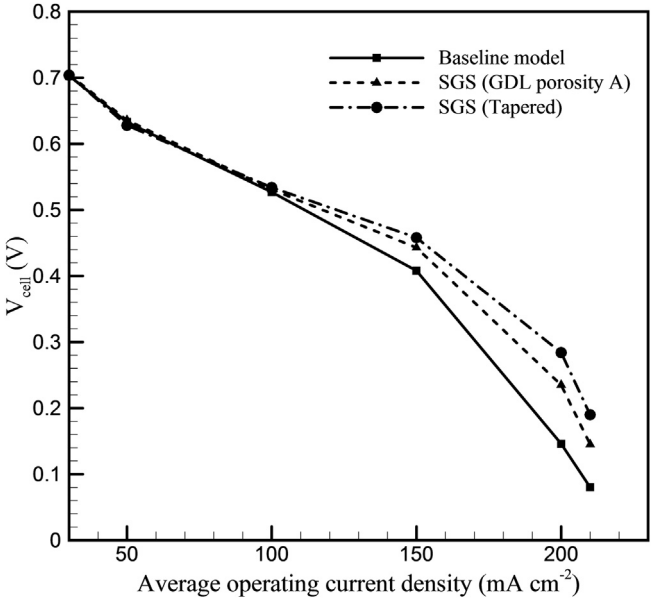

Fig. 14. Comparison of polarization curves of DMFCs.

List of symbols

Acronyms and abbreviations

A	area (m^2)
a_s	specific reaction are (m^{-1})
C	molar concentration (mol m^{-3})
D	diffusivity (m^2 s^{-1})
D_H	Hydraulic diameter (m)
E^0	thermodynamic reversible voltage (V)
H	channel height (m)
h_m	convective mass transfer coefficient
I	current (A)
i	current density (A m^{-2} or mA cm^{-2})
$i_{0,a}$	Anode exchange current density (A m^{-2})
$i_{0,c}$	Cathode exchange current density (A m^{-2})
j	mass flux (kg m^{-2} s^{-1}), phase diffusion flux (mol m^{-2} s^{-1}), volumetric transfer current density (A m^{-3})
$\vec{j}$	phase diffusion flux (mol m^{-2} s^{-1}),
K	permeability (m^2)
k_a	anode kinetics coefficient
k_H	Henry's constant
L	channel length (m)
m	mass (kg)
M	molar weight (g mol^{-1})
N	molar flux (mol m^{-2} s^{-1})
p	pressure (Pa)
n_d	electro-osmosis drag coefficient
s	liquid saturation, entropy
S	volumetric source term
u	velocity (m s^{-1})
U^0	open circuit voltage (V)
T	temperature (K)
Y	species mass fraction

Greek letters

α	water transfer coefficient, void fraction, transfer number
ε	porosity
δ	thickness
κ	ionic conductivity
ρ	density
τ	shear stress
γ	advection correction factor
η	overpotential, efficiency
Φ	potential
θ	angle
λ	mobility, water content
σ	surface tension
μ	viscosity
ω	catalyst loading amount (g cm^{-2})

Superscript and subscript

a	anode
abp	anode bipolar plate
acl	anode catalyst layer
agdl	anode gas diffusion layer
ampl	anode micro-porous layer
c	cathode
capill	capillary
cbp	cathode bipolar plate
ccl	cathode catalyst layer
cgdl	cathode gas diffusion layer
chan	channel
cl	catalyst layer
cmpl	cathode micro-porous layer
D	drag
diff	diffusion
e	electrolyte phase
eff	effective
g	gas
gdl	gas diffusion layer
int	interfacial
k	species
l	liquid
mem	membrane
ref	reference
s	solid phase
tot	total
xover	crossover

References

[1] A. Blum, T. Duvdevani, M. Philosoph, N. Rudoy, E. Peled, J. Power Sources 117 (2003) 22.
[2] G.Q. Lu, P.C. Lim, F.Q. Liu, C.Y. Wang, Int. J. Energy Res. 29 (2005) 1041.
[3] G.Q. Lu, C.Y. Wang, J. Fuel Cell Sci. Tech. 3 (2006) 131.
[4] Z.H. Wang, C.Y. Wang, J. Electrochem. Soc. 150 (2003) A508.
[5] W. Liu, C.Y. Wang, J. Electrochem. Soc. 154 (2007) B352.
[6] S. Jung, J. Power Sources 231 (2012).
[7] C.Y. Wang, P. Cheng, Int. J. Heat Mass Transfer 39 (17) (1996) 3607.
[8] F.P. Incropera, D.P. DeWitt, Fundamentals of Heat and Mass Transfer, Fifth ed., 2002.
[9] J.P. Meyers, J. Newman, J. Electrochem. Soc. 149 (2002) A710.
[10] J.P. Meyers, J. Newman, J. Electrochem. Soc. 149 (2002) A718.
[11] J.P. Meyers, J. Newman, J. Electrochem. Soc. 149 (2002) A729.
[12] U. Pasaogullari, C.Y. Wang, Electrochem. Acta 49 (2004) 4559.
[13] F. Liu, C.Y. Wang, Electrochem. Acta 53 (2008) 5517.
[14] R.H. Brooks, A.T. Corey, Hydrology Papers, 3, Colorado State University, 1964, p. 1.
[15] R.B. Mrazek, C.E. Wicks, K.N.S. Prabhu, J. Chem. Eng. Data 13 (1968) 508.
[16] B.E. Poling, J.M. Prausnitz, J.P. O'Connell, The Properties of Gases and Liquids, fifth ed., McGraw-Hill, New York, 2001.
[17] T.E. Springer, T.A. Zawodzinski, S. Gottesfeld, J. Electrochem. Soc. 138 (1991) 2334.
[18] T.A. Zawodzinski, C. Derouin, S. Radzinski, R.J. Sherman, V.T. Smith, T.E. Springer, S. Gottesfeld, J. Electrochem. Soc. 140 (1993) 1041.
[19] G. Lu, C.Y. Wang, An Invited Chapter for New Developments in Heat Transfer (Chapter 9), 2005, p. 317.
[20] Z.J. Derlacki, A.J. Easteal, V.J. Edge, L.A. Woolf, Z. Roksandic, J. Phys. Chem. 89 (1985) 5318.
[21] T.A. Zawodzinski, J. Davey, J. Valerio, S. Gottesfeld, Electrochem. Acta 40 (1995) 297.